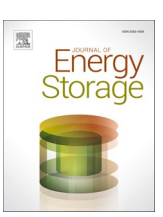
ELSEVIER

Contents lists available at ScienceDirect

## Journal of Energy Storage

journal homepage: www.elsevier.com/locate/est



## Research papers



# Advancing ionic conductivity in solid electrolytes: Insights from polymerization-induced phase separation and microstructural optimization

Nasser Nikfarjam<sup>a</sup>, Paul T. Coman<sup>a,\*</sup>, Colton Free<sup>a</sup>, Paul Ziehl<sup>b</sup>, Monirosadat Sadati<sup>a,\*</sup>, Ralph E. White<sup>a</sup>

- a Department of Chemical Engineering, University of South Carolina, Columbia 29208, SC, USA
- <sup>b</sup> Department of Civil and Environmental Engineering, University of South Carolina, Columbia 29208, SC, USA

#### ARTICLE INFO

#### Keywords: Lithium-ion battery Polymerization-induced phase separation Solid polymer electrolyte Porosity Ionic conductivity

#### ABSTRACT

This study aims to present a comprehensive experimental analysis of the polymerization-induced phase separation (PIPS) in solid polymer electrolytes. This process is key to developing polymer membranes with enhanced ionic conductivity, where phase separation plays a critical role in facilitating ions transport through the electrolyte matrix. We synthesized heterogeneous electrolyte membrane (HEM) films utilizing a thermally initiated PIPS approach. In this process, Bisphenol-A ethoxylate dimethacrylate (BPA-EDMA) served as the monomer, which was polymerized in the present of dimethyl methylphosphonate (DMMP) and ethylene carbonate (EC) solvents, and lithium trifluoromethanesulfonate (LiTFS) salt. We performed comprehensive rheological, morphological, and mechanical analyses to assess the effect of monomer concentrations and LiTFS salt levels on the polymerization and phase separation processes and understand their subsequent impact on ionic conductivity.

Our results underscore the intricate connection between the ionic conductivity of HEMs and their microstructure and mechanical properties, which are significantly affected by the monomer and salt concentrations. The highest porosity in the polymer membranes was obtained for a solution with 40 wt% monomer and 1 M salt, yet the best ionic conductivity was measured in membrane containing 50 wt% monomer and 1 M salt, which exhibited increased mechanical stiffness. These observations underline the critical balance needed between porosity and structural integrity for optimal ionic conductivity performance. Further increases in these concentrations led to densely crosslinked polymer networks, which adversely affected ionic conductivity. These findings, corroborated by rheological characterizations, confirm that monomer and salt content significantly influence the phase separation dynamics. Furthermore, Flory–Huggins mean–field theory offers a theoretical perspective to interpret these experimental observations, thereby contributing to a deeper understanding of the interplay between chemical composition, structural properties, and functional performance in polymer-based solid electrolytes. This study enhances our fundamental knowledge for developing materials with tailored ionic conductivity.

## 1. Introduction

With more and more Electrical Vehicles (EVs) protruding into the global market, a large amount of attention has been drawn to Li-ion batteries, both in industry and in government agencies. Large funding has been dedicated to improving Li-ion batteries, including improvements to the energy density, safety, cycle life, etc. Scientists all over the world are exploring innovative alternatives to traditional Li-ion batteries, which use a liquid electrolyte, by developing solid-state batteries.

These alternatives promise enhanced safety and greater flexibility in designing various shapes. One such alternative is structural batteries, comprising a bare carbon fiber anode, an electroactive-coated carbon fiber cathode, and a solid electrolyte sandwiched between them. These batteries have the potential to decrease system weight while providing structural strength.

Liquid electrolytes have traditionally been utilized for high Li-ion transfer in the electrolyte with ionic conductivity. These electrolytes usually exhibit high energy density and excellent rate capability [1,2].

<sup>\*</sup> Corresponding authors at: Department of Chemical Engineering, University of South Carolina, Columbia, SC 29208, USA. E-mail addresses: comanpt@cec.sc.edu (P.T. Coman), sadati@cec.sc.edu (M. Sadati).

However, liquid electrolytes have a weakness in providing thermal stability, flexural strength, electrochemical stability, and Li dendrite suppression. Moreover, the flammability and leakage risks of liquid electrolytes have led to safety concerns. Therefore, in batteries where structural strength and safety are essential, such as structural batteries, the use of solid electrolytes is crucial [3]. Over the years solid-based electrolytes have been developed in different forms, whether ceramic, oxide, or polymer-based, while the latter is preferable for composite systems like structural batteries. The polymer-based electrolytes are of different types, such as Solid Polymer Electrolyte (SPE), Gel Polymer Electrolyte (GPE), Composite Solid Polymer Electrolyte (CSPE), and Heterogeneous Electrolyte Membrane (HEM).

SPE are made of a soft polymer to diminish leakage issues and enhance dimensional stability [4]. Among these types, poly(ethylene oxide) (PEO) has been a prominent candidate for SPE fabrication, where soft PEO segments can coordinate Li ions to enhance ionic conductivity [5]. However, considering that the PEO crystallization suppresses the ionic conductivity, slightly crosslinking of PEO has been proposed to reduce crystallization possibility and provide an enhanced ionic conductivity [6–8]. However, the higher the crosslinking degree, the higher the mechanical strength (elastic modulus  $\sim$ 100 MPa), and the lower ionic conductivity ( $\sim$ 10<sup>-6</sup> S cm<sup>-1</sup>) [2,9–12].

In GPE, the incorporation of solvent molecules into the polymeric solid electrolyte, plasticizes the polymer chains and enhances the ionic conductivity [5,13]. Although the ionic conductivity is improved significantly ( $\sim 10^{-2} \, \mathrm{S \, cm^{-1}}$ ), their mechanical features are considerably diminished, limiting their practical applications as structural batteries [2,13].

CSPEs are built by introducing nano-scale reinforcement (e.g., aerogel and cellulose nanofibril, etc.) into the polymeric electrolyte. This two-phase system design improves mechanical performance [14,15]. However, it is well recognized that there exists a reciprocal relationship between ionic conductivity and mechanical performance, as rigidity does not require molecular mobility, whereas ionic conductivity does [16–18]. Therefore, finding nanoscale reinforcing agents that enhance both mechanical properties and conductivity is somewhat challenging.

HEM, as another alternative of heterogenous structures, consists of at least two material phases to create submicron-scale percolating structures. In the liquid-polymer HEMs, the solid polymer phase provides the three-dimensional structure and mechanical strength, while the liquid phase, as a mobile phase, can provide ionic conductivity. HEMs can be fabricated using the polymerization-induced phase separation (PIPS) process. In this process, initially miscible monomers and solvents phase separate into polymer-rich and solvent-rich regions as polymerization advances, resulting in an interconnected bi-continuous structure [19,20]. The phase separation phenomenon is influenced by various factors such as difference between the solubility parameter of components, polymerization temperature, type (free radical or polycondensation), and kinetics. PIPS can be initiated by UV [21,22] or thermal initiators [19,20]. However, the UV method is not applicable for structural battery preparations, where multiple opaque layers of material are involved, acting as a barrier against UV irradiation penetration. In comparison, thermal energy can be distributed homogeneously throughout the system and initiate PIPS simultaneously.

Various epoxy and vinyl ester resins or monomers have been used to fabricate HEMs through the PIPS method for Li-battery applications. For example, Manly et al. prepared a porous membrane via UV-curing of 1,4-butanediol diacrylate in ethylene carbonate for 10 minutes [23]. Sakakibara et al. utilized a derivative of bis(diglycidylaminoethyl) cyclohexane as a monomer and bis(aminocyclohexyl)methane as a crosslinking agent which were polymerized at different temperatures (70–130 °C) for 1 h to synthesize mesoporous monolith membrane [24]. Song et al. fabricated flexible HEMs using diglycidyl ether of bisphenol-A and methyl tetrahydrophthalic anhydride as crosslinking agents [25]. Ihrner et al. [21], Schneider et al. [26], and Cattaruzza et al. [27], prepared porous membranes through both UV- and thermal-initiated

PIPS of bisphenol-A ethoxylate dimethacrylate (BPA-EDMA) with different molecular weights. In their works, ethylene carbonate (EC, with a solubility parameter of 30.1 MPa<sup>1/2</sup>) and dimethyl methylphosphonate (DMMP, with a solubility parameter of 23.72 MPa<sup>1/2</sup>) were used as a good solvent for BPA-EDMA monomers which phase separated over the polymerization process [28–30]. These monomers have been specifically designed for fabricating HEMs in Li-battery applications, with most studies primarily focused on enhancing the ionic conductivity of HEMs. However, there is limited understanding of how the phase separation mechanism contributes to the ionic conductivity of the final structures.

In this study, we will utilize a range of complementary characterization techniques, encompassing thermal, rheological, imaging, and conductivity analyses, to investigate the structural evolution during the PIPS process and its influence on the ionic conductivity of HEMs. HEMs are synthesized based on bisphenol-A ethoxylate dimethacrylate (BPA-EDMA) through the thermal-initiated PIPS process. We explore the effect of monomer content and lithium salt on the PIPS mechanism by performing rheological characterizations of the reactive electrolyte solutions during polymerization and morphological analysis of the structures after polymerization. Ultimately, we will assess the ionic conductivity of the membrane to understand the relationship between its microstructure and ionic conductivity, considering its potential as a solid electrolyte for Li-ion battery applications.

### 2. Experimental

#### 2.1. Materials

Bisphenol A ethoxylate dimethacrylate (BPA-EDMA,  $\overline{M}_n=540~{\rm g\cdot mol}^{-1}$ ), dimethyl methylphosphonate (97 %) (DMMP), ethylene carbonate (99 %, anhydrous) (EC), 2,2′-azobis(2-methylpropionitrile) (AIBN, thermal initiator), and lithium trifluoromethanesulfonate (LiTFS) (96 %) were purchased from Sigma-Aldrich and used as received.

## 2.2. Heterogeneous electrolyte membrane (HEM) fabrication

Two series of liquid electrolyte solutions, with different monomer and Li-based salt concentrations (LiTFS-type) were prepared, as described in Table 1. To examine how the monomer influences the membrane's characteristics, the content of BPA-EDMA was progressively altered, ranging from 20 to 70 wt%, with increments of 10 % at each step. To assess the impact of the salt, the concentration of LiTFS was adjusted in increments of 0.5 M, ranging from 0 M (no salt) to 1.5 M.

The stock solution was first prepared by mixing the two solvents DMMP and EC in a weight ratio of 1:1 (i.e., DMMP:EC = 50:50 wt%) for all the electrolyte solutions. Next, LiTFS salt was added to the solution and stirred until complete dissolution. Subsequently, the BPA-EDMA and AIBN were added to the solution and stirred for at least 30 min for complete dissolution. Finally, AIBN as an initiator was introduced to the solution according to Table 1 to prepare the final liquid electrolyte solutions. All solutions were prepared in a glovebox, under argon atmosphere and dry conditions ( $O_2 < 0.5$  ppm). For post-polymerization analysis, the membrane films were labeled as  $M_x$ -Li $_y$ , where x and y indicate their monomer content (wt%) and LiTFS concentration (M), respectively.

For the HEM fabrication, the thermal polymerization of the liquid electrolyte solutions was performed in glass cells having the gap thicknesses of 50, 100, 200, and 400  $\mu$ m. The prepared liquid electrolytes were gently added with a dropper, and the solutions permeated into the glass cell due to the capillarity forces (Fig. 1). The glass cell was then sealed thoroughly and transferred to an oven and cured at 60 °C for 4 h. During the polymerization process, the colorless liquid electrolytes in most samples transformed into solid white membrane films, indicating

**Table 1**The chemical composition of the HEM samples.

	Samples	BPA-EDMA, g (wt% <sup>a</sup> )	EC, g	DMMP, g	DMMP/EC, weight ratio	LiTFS, M	BPA-EDMA/AIBN, molar ratio
	M <sub>20</sub> -Li <sub>1.0</sub>	0.358 (20)	0.635	0.635	1	1.0	47
	$M_{30}$ -Li <sub>1.0</sub>	0.635 (30)	0.635	0.635	1	1.0	47
	$M_{40}$ -Li <sub>1.0</sub>	0.954 (40)	0.635	0.635	1	1.0	47
	$M_{50}$ -Li <sub>1.0</sub>	1.432 (50)	0.635	0.635	1	1.0	47
	$M_{60}$ -Li <sub>1.0</sub>	2.200 (60)	0.635	0.635	1	1.0	47
	$M_{70}$ -Li <sub>1.0</sub>	3.340 (70)	0.635	0.635	1	1.0	47
LiTFS Series	$M_{40}$ -Li <sub>0.0</sub>	0.954 (40)	0.635	0.635	1	0.0	47
	$M_{40}$ -Li <sub>0.5</sub>	0.954 (40)	0.635	0.635	1	0.5	47
	$M_{40}$ -Li <sub>1.0</sub>	0.954 (40)	0.635	0.635	1	1.0	47
	$M_{40}$ -Li <sub>1.5</sub>	0.954 (40)	0.635	0.635	1	1.5	47

<sup>&</sup>lt;sup>a</sup> The values in parentheses show the monomer weight percent based on the total weight of components in the solution.

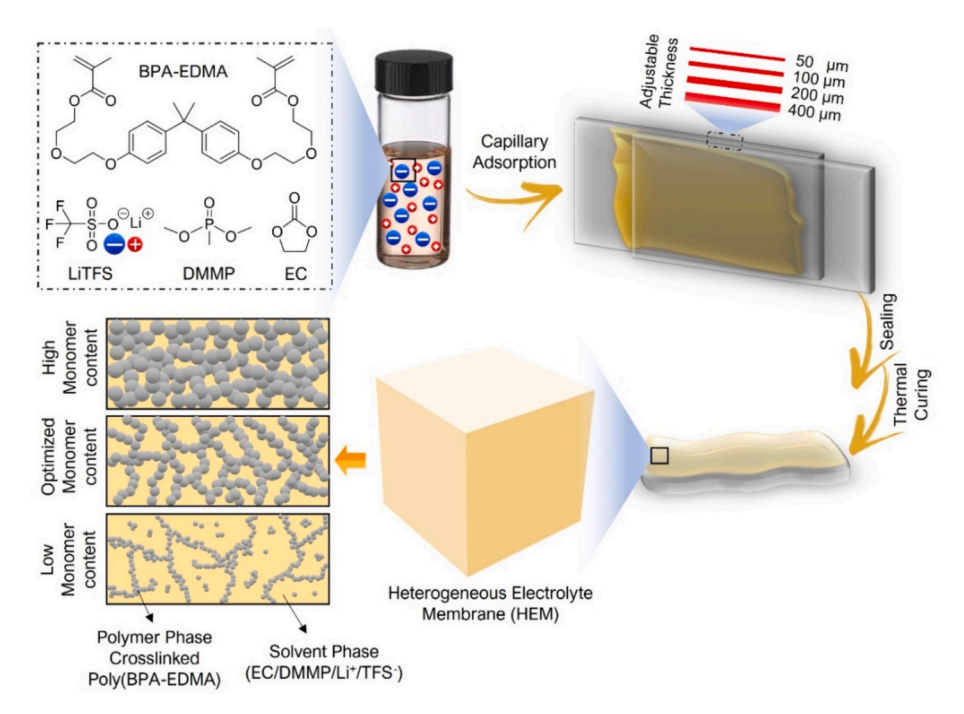


Fig. 1. Illustration of the steps carried out to fabricate the heterogeneous electrolyte membrane (HEM).

the occurrence of phase separation. After the polymerization, the HEM films were peeled from the glass cells for further characterization.

## 2.3. Characterization

### 2.3.1. Field-Emission Scanning Electron Microscopy (FE-SEM)

The microstructure and morphology of HEM films were explored by SEM imaging. The surface and cross-section views of the HEM films for both monomer and LiTFS series were investigated using a Zeiss Gemini500 FE-SEM operating at 5.0 kV. All the films were immersed in deionized water twice and each time for 12 h to remove the LiTFS, EC, and DMMP. Subsequently, the films were dried in a vacuum oven at 50  $^{\circ}\text{C}$  for 24 h. The samples and related fractured sections were vacuum coated with a thin layer of gold before imaging.

#### 2.3.2. In-situ rheometry of liquid electrolytes during polymerization

To study PIPS kinetics, the rheological behavior of the prepared reactive liquid electrolytes for both series was monitored during the polymerization using a Discovery Hybrid (HR-2) Rheometer equipped with a flat stainless-steel plate with a diameter of 40 mm. The liquid electrolyte (640  $\mu L)$  was injected between two parallel plates and oscillatory sweep tests were performed with a plate gap of 500  $\mu m$ , angular frequency of 10 rad/s, and strain of 0.1 % at 60 °C for 2 h. A solvent trap was used to avoid any solvent evaporation during the

polymerization.

#### 2.3.3. Tensile testing

The mechanical properties of the HEM films were characterized using the tensile test geometry on Discovery Hybrid (HR-2) Rheometer. The test specimens measured 25 mm in length, 10 mm in width, and 0.1 mm in thickness and the tensile force was loaded at a rate of  $10~\mu m/min$ . The average nominal elastic modulus (Young's modulus), tensile stress, and elongation at break were determined from the tensile stress–strain curves using Origin2021b Pro software. The nominal stress was obtained by dividing the tensile force by the initial cross-sectional area of the specimen.

## 2.4. Coin cell preparation

For the ionic conductivity measurements, Li | Li symmetrical coin cells (using the reversible-electrode method, as seen in Fig. 2A) were prepared in an Argon-filled glove box (a maximum oxygen concentration of 0.5 ppm). First, a 16 mm lithium metal disk-shaped electrode was placed in the stainless-steel bottom can, followed by the prepared disk-shaped HEM film with a diameter of 19 mm and various thicknesses, and then another 16 mm disk-shape lithium metal, a spacer disk, a wave washer, the coin cell insulating gasket, and finally the positive stainless-steel cell cap (Fig. 2A). The assembled coin cell was crimped inside the

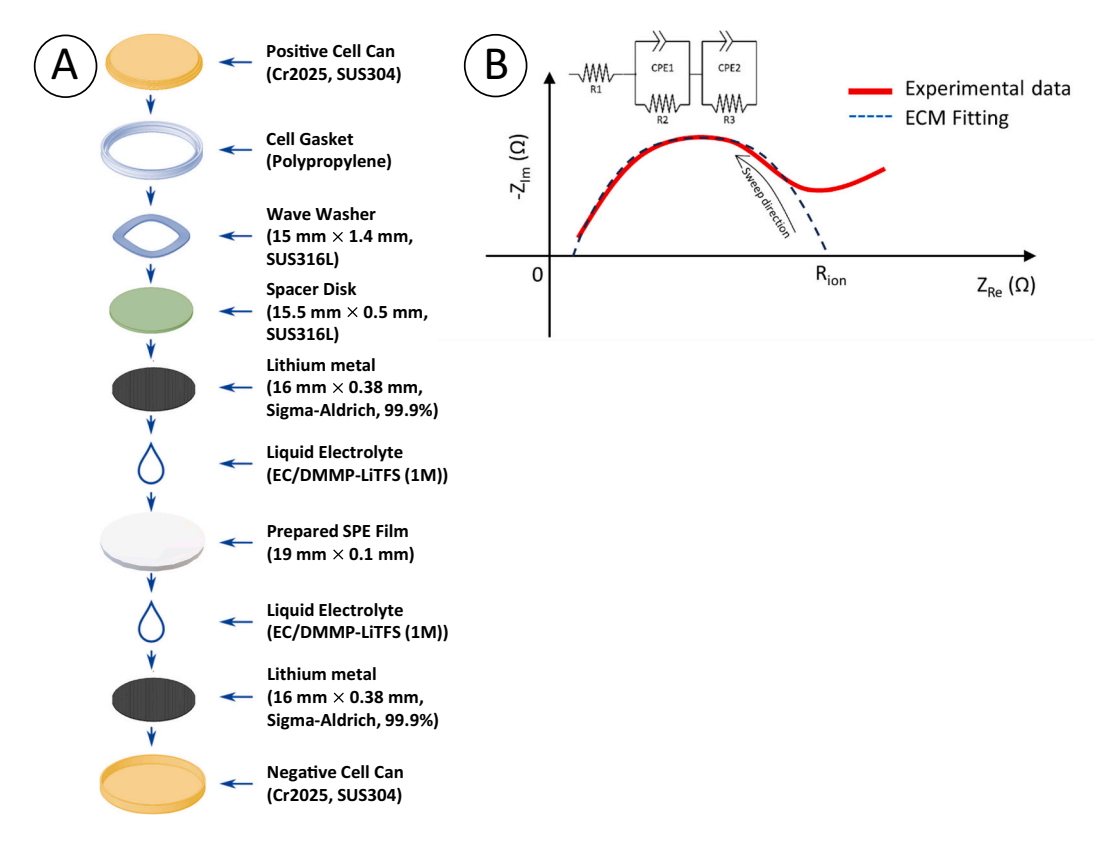


Fig. 2. (A) Assembly flow diagram demonstrating the Li | Li symmetrical coin cell configurations used for measuring the ionic conductivity. (B) Sample of Nyquist plot used to determine the ionic conductivity by fitting an equivalent circuit and using the point where the curve intercepts  $Z_{im} = 0$ .

glove box and then taken out for electrochemical characterization. Two types of coin cells were prepared. i) the assembled coin cells included the HEM films prepared by electrolyte solutions containing different amounts of monomer (40, 50, 60, and 70 wt%, Table 1) at constant 1 M LiTFS concentration (M<sub>40</sub>-Li<sub>1.0</sub>, M<sub>50</sub>-Li<sub>1.0</sub>, M<sub>60</sub>-Li<sub>1.0</sub> and M<sub>70</sub>-Li<sub>1.0</sub>). It is worth noting that the samples with lower monomer contents (<40 %) did not provide integrated HEM films. ii) the coin cells based on the prepared HEMs with a 50 wt% of monomer content and 1 M LiTFS concentrations with extra added electrolyte solution 1 M LiTFS EC/DMMP(50:50) in different volume amounts (0, 4, 10, and 20  $\mu L$ , divided on each side of the membrane), denoted with M<sub>50</sub>-Li<sub>1.0</sub>-S<sub>0</sub>, M<sub>50</sub>-Li<sub>1.0</sub>-S<sub>4</sub>, M<sub>50</sub>-Li<sub>1.0</sub>-S<sub>10</sub>, and M<sub>50</sub>-Li<sub>1.0</sub>-S<sub>20</sub>.

## 2.5. Ionic conductivity measurements of the prepared coin cells

The Electrochemical Impedance Spectroscopy (EIS) technique was used to determine the ionic conductivity of each film, with measurements conducted using a WaveDriver 200 EIS Bipotentiostat from Pine Instruments in Galvanostatic Mode. Once extracted from the glove box, the coin cells were inserted in a Battery Coin-Cell Holder from Arbin, and the four leads from the holder were connected to the instrument (a Working Electrode, Sense lead, Reference, and Counter Electrode). For each cell/sample, the impedance was measured in the frequency range from 1 Hz to 300 kHz (see the Sweep direction in Fig. 2), with an amplitude of  $1000\,\mu\text{A}$  and a 5 points per decade resolution. For each coin cell, a Nyquist plot was obtained and data was fitted using the equivalent circuit from Fig. 2B to determine the point where the low-frequency part of the curve (to the right) intersects the 0 imaginary impedance [31].

The ionic conductivity was calculated using the following equation:

$$\sigma_{M_x - Li_y} = \frac{l_{film}}{R_{ion} A_{film}} \tag{1}$$

where  $\sigma$  is the ionic conductivity of the film,  $l_{\text{film}}$  is the thickness of the

film,  $R_{\rm ion}$  is the ionic resistance of the film and A is the cross-sectional area of the contact between the lithium disks and the polymer (A  $\approx 2.011~{\rm cm}^2$ ). Considering that there might be some variability in the way the cells were crimped, in some cells the real resistance was shifted to the right, therefore,  $R_{\rm ion}$  is calculated by subtracting the point where it intersects the 0 imaginary to the right and the point where it intersects 0 on the left, in the high-frequency area, to reduce the influence of residual resistances. The thickness and the width of each HEM film were measured with a digital slide caliper.

The AC impedance and the ionic conductivity, respectively, were measured and calculated at ambient temperature on the two series of prepared coin cells.

#### 3. Result and discussion

#### 3.1. Materials characterization

BPA-EDMA with 2 ethylene oxide repeating units at both sides of BPA was used as a monomer in the present study (Fig. 1). The BPA core with hydrophobic nature imparts rigidity to the final HEM film. In contrast, the polar ethylene oxide units contribute to flexibility, ionic conductivity, and the ability to accommodate lithium salt, enhancing the overall performance of the films. Additionally, ethene oxide segments enhance the solubility of BPA-EDMA monomer in the selected polar solvent mixtures (i.e., EC:DMMP). Two series of electrolyte liquids were prepared to determine the effect of BPA-EDMA monomer and LiTFS salt contents on the HEM's structural morphology, mechanical properties, and ionic conductivity. In the monomer series, the BPA-EDMA monomer content was varied from 20 to 70 wt% based on the total weight of the components, as seen in Table 1. In the LiTFS series, the effect of LiTFS concentrations was examined within the range of 0 to 1.5 molar, while maintaining a constant BPA-EDMA content of 40 wt% based on the volume of the EC:DMMP solvent mixture. Subsequently,

HEM films corresponding to these solutions were synthesized by injecting the liquid into a pre-prepared glass cell with varying gaps. The cell was then sealed and subjected to a curing process at 60 °C for a period of 4 h. During the polymerization, the solutions that were initially transparent gradually turned opaque and white, indicating structural transformation and the onset of phase separation. In fact, the mixture of EC:DMMP solvents dissolves the BPA-EDMA monomer entirely indicating their similar solubility parameter. However, following polymerization, the difference in solubility parameters between the newly formed poly(BPA-EDMA) and EC:DMMP solvent increases, resulting in the phase separation of the mixture into a bi-continuous network of two distinct i) a polymer-rich phase containing solid poly(BPA-EDMA) and ii) solution-rich phase of EC/DMMP/LiTFS. In the early stages of polymerization, polymer chains are gradually formed and separated from the liquid solvents to generate polymer-rich and polymer-lean regions. This process of PIPS results in the formation of a three-dimensional bicontinuous network comprising polymer and solvent, where the solid interconnected polymeric network (stationary phase) provides dimensional and mechanical stability for the polymeric membrane, while the solvent phase within the porous interconnected channels provides a mobile phase for Li ion transportation [19,32].

At low monomer concentrations (30 wt% and below), polymerization of the reactive liquid electrolytes resulted in the formation of HEM films with insufficient structural stability and mechanical integrity (Fig. S1, below <30 wt% the films fall apart upon detachment from the sample cell). Increasing the monomer content in the reactive electrolyte solutions from 40 to 70 wt% led to the formation of uniform solid but

flexible polymer membranes with higher mechanical integrity.

To gain a deeper insight into the influence of monomer content on the phase separation process and structural porosity, the solvents and LiTFS were extracted from the membrane films, and the structural morphology of the resulting dried membranes was examined using FE-SEM imaging. The FE-SEM images of the sample containing 30 wt% of BPA-EDMA (M<sub>30</sub>-Li<sub>1.0</sub>) revealed the presence of large cracks on the membrane surface caused by the insufficient monomer content and, thus, the inadequate solid polymer network. An integrated porous structure was achieved as the monomer content increased from 40 to 70 wt%. Nevertheless, there was a decrease in pore size (or channel diameter) as the monomer content increased (Fig. 3A). Notably, films with higher monomer content exhibited increasing transparency compared to those with lower monomer content (compare M<sub>70</sub>-Li<sub>1.0</sub> with M50-Li1.0 and M40-Li1.0 in Fig. S1). The reduction in pore size at high monomer content can be attributed to i) the enhanced viscosity of liquid electrolyte, reducing system's dynamics and hindering polymer chain diffusion from polymer-lean phase to polymer-rich phase and resulting in incomplete phase separation, and ii) rapid crosslinking kinetics due to the high monomer content, arresting the phase separation process at the early stages [21]. This latter also explains why the membrane films prepared with highest monomer contents exhibited greater transparency than those with lower (Fig. S1).

In the LiTFS series, the monomer content was kept at 40 wt%, and LiTFS concentration varied from 0 to 0.5, 1.0, and 1.5 M (Table 1). For the sample  $M_{40}$ -Li $_{0.0}$ , which contains no LiTFS, the FE-SEM images revealed a microscale porous network structure with large pore sizes.

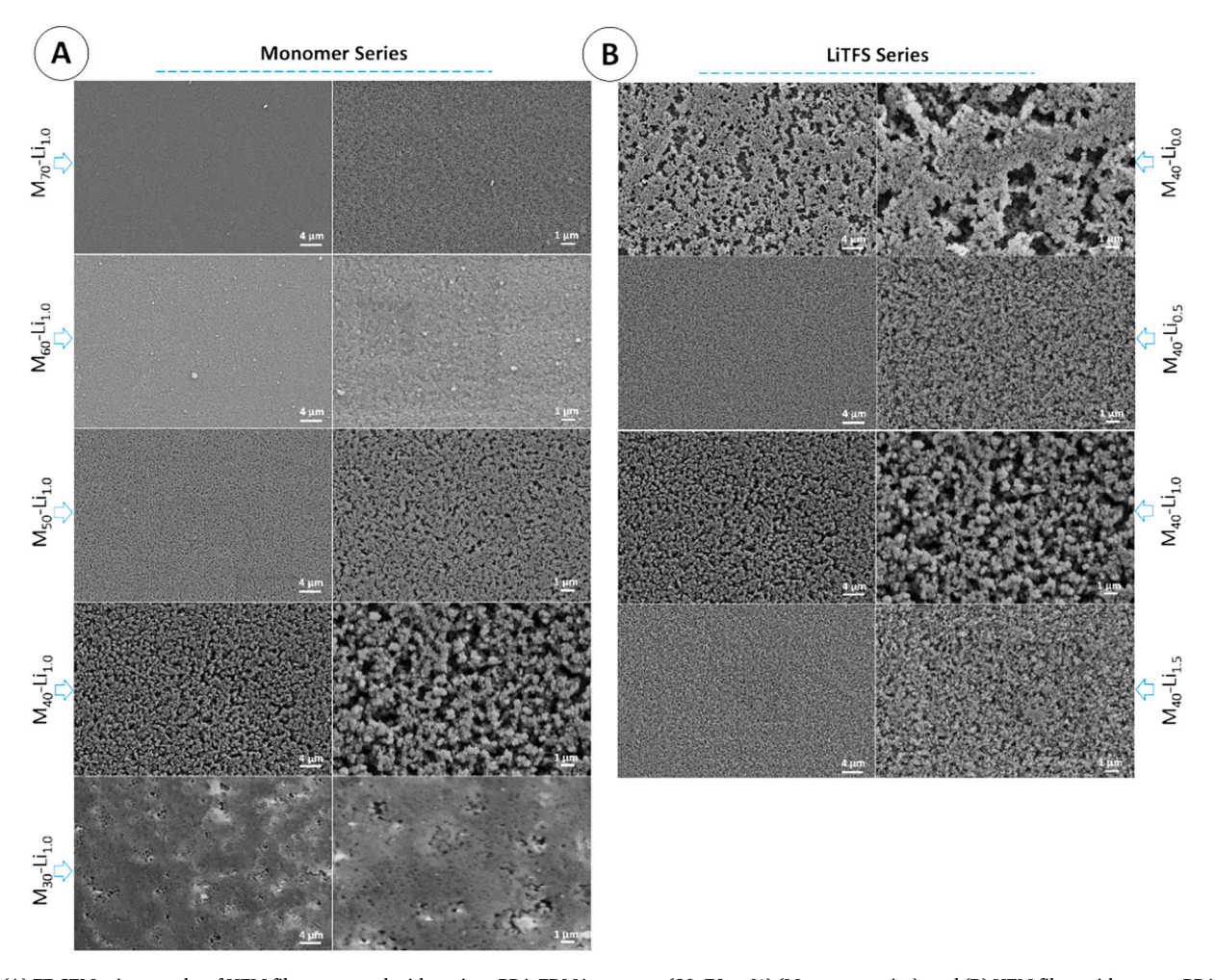


Fig. 3. (A) FE-SEM micrographs of HEM films prepared with various BPA-EDMA contents (30–70 wt%) (Monomer series), and (B) HEM films with a same BPA-EDMA content of 40 wt%, but different LiTFS concentrations (0–1.5 M) (LiTFS series).

However, adding LiTFS at 0.5 M significantly eliminated the discrete pores, reducing their size, forming finely phase-separated bi-continuous network morphology (compare  $M_{40}$ -Li $_{0.0}$  and  $M_{40}$ -Li $_{0.5}$  in Fig. 3B). The pore size increased with further addition of LiTFS from 0.5 M to 1.0 M ( $M_{40}$ -Li $_{0.5}$  and  $M_{40}$ -Li $_{1.0}$  in Fig. 3B). Adding more LiTFS, specifically in the  $M_{40}$ -Li $_{1.5}$  composition, led to a further reduction in pore size (Fig. 3B). This suggests that at increased LiTFS concentrations, the degree of phase separation becomes less pronounced.

To investigate the effect of the thickness of the membrane on the structural morphology, four membranes with various thicknesses (50, 100, 200, and 400  $\mu m$ ) were prepared at the same monomer and salt composition (40 wt% monomer content and 1 M LiTFS –  $M_{40}\text{-Li}_{1.0}$ ). The FE-SEM images obtained from the surface and cross-sectional views of the films showed that all samples had a relatively homogeneous porous structure, and no significant changes in the morphology of the films were observed (Fig. 4A–B). One can conclude that i) polymerization and phase separation are uniform through the thickness and ii) composition (i.e., BPA-EDMA and LiTFS contents) plays a crucial role in defining the morphology of the films rather than the thickness.

#### 3.2. Phase separation theory

The significant dependency of the membrane films' structural morphology on the monomer content and LiTFS concentration relies on the intermolecular interaction changes between the formed polymer chains (poly(BPA-EDMA)) and electrolyte solution components during the PIPS process. The polymer phase separation can be explained analytically through the Flory-Huggins mean-field theory in terms of the binary mixing free energy change ( $\Delta G_{mix}$ ) of the polymer solution [33,34], where, poly(BPA-EDMA) and solvent (and salt) species (EC, DMMP, and LiTFS) are components 1 and 2 of the binary polymer

solution during PIPS through free radical polymerization. The Gibbs free energy change can be calculated as follows [33]:

$$\Delta G_{mix} \approx kT \left( \frac{\phi_1}{x_1} ln \phi_1 + \frac{\phi_2}{x_2} ln \phi_2 + \chi \phi_1 \phi_2 \right)$$
 (2)

where k is the Boltzmann constant, and T is the absolute temperature.  $\phi$  ( $0 \le \phi \le 1$ ), and x are the volume fractions of the components in the mixture, and the degree of polymerization, respectively. Since  $x_2 = 1$  for solvents, Eq. (2) becomes:

$$\Delta G_{mix} \approx kT \left( \frac{\phi_1}{x_1} ln \phi_1 + \phi_2 ln \phi_2 + \chi \phi_1 \phi_2 \right)$$
 (3)

In Eqs. (2) and (3),  $\chi$  is the Flory–Huggin's interaction parameter, which is proportional to the solubility parameter difference ( $\Delta\delta$ ) of components by the following equation:

$$\chi = \frac{\overline{V}_1}{RT}(\delta_1 - \delta_2)^2 \tag{4}$$

where,  $\overline{V}_1$  and R are the partial molar volume and the universal gas constant, respectively. Therefore, in Eq. (2),  $(\phi_1 ln\phi_1)/x_1$  and  $\phi_2 ln\phi_2$  are considered as the first and second entropy terms, and  $\chi\phi_1\phi_2$  is considered as enthalpy term.

With the salt concentration held constant, as the polymerization progresses and  $x_1$  increases, the system's entropy  $((\phi_1ln\phi_1)/x_1)$  decreases. Concurrently,  $\chi$  and hence the enthalpy  $(\chi\phi_1\phi_2)$  become more significant, attributed to the growing difference in solubility parameter difference  $(\Delta\delta)$  between the solvent (EC/DMMP) and the polymer chains. These decrease in entropy and increase in enthalpy over polymerization will lead to more positive  $\Delta G_{mix}$  driving the phase separation of the system into two polymer-rich and solvent-rich phases. Hence, it

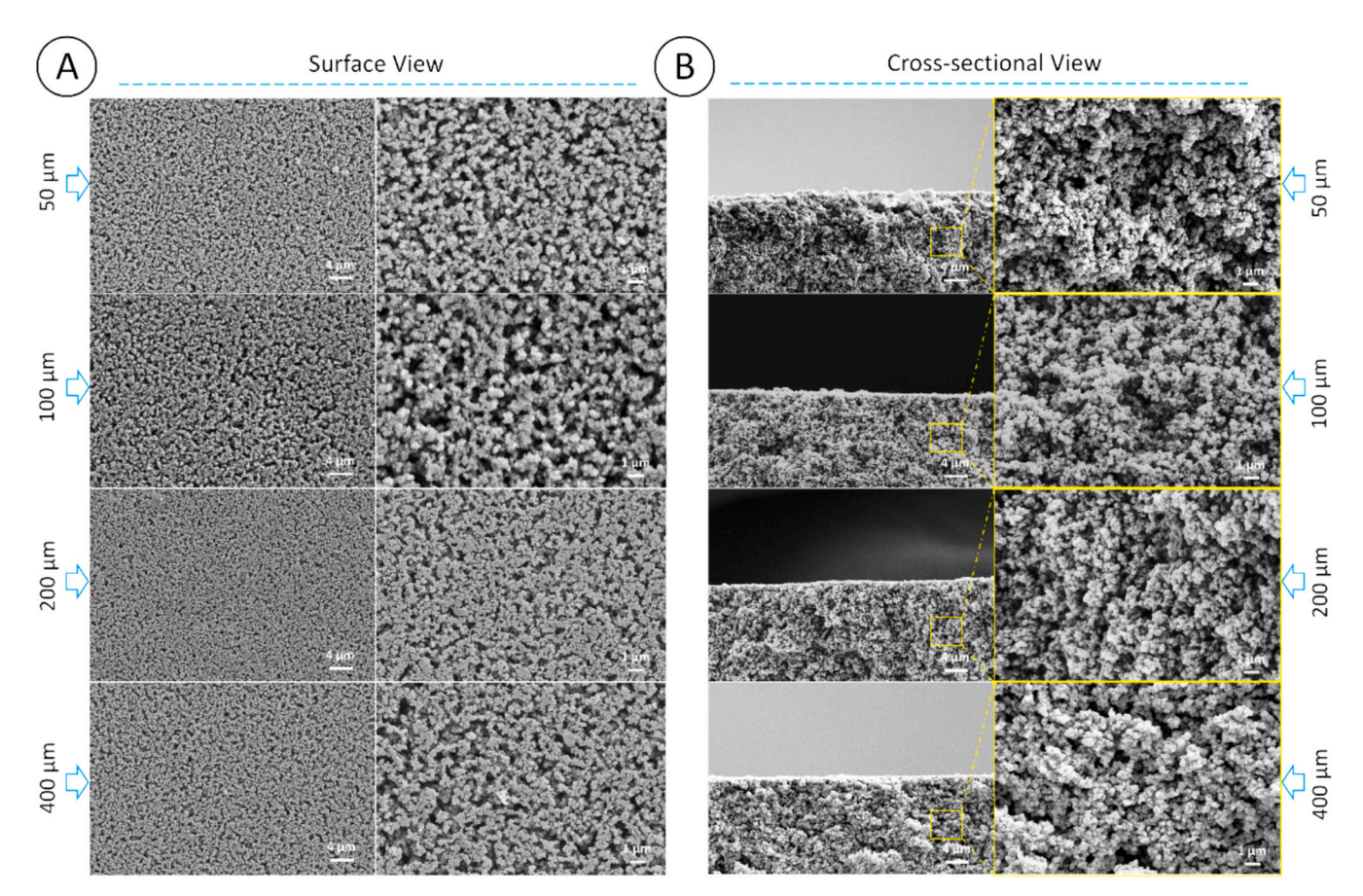


Fig. 4. (A–B) Surface and cross-section FE-SEM micrographs of  $M_{40}$ -Li<sub>1.0</sub> samples prepared at different thicknesses (50–400  $\mu$ m).

can be concluded that the polymerization degree (x) and Flory–Huggin's interaction parameter ( $\chi$ ) are two critical factors in the PIPS phenomenon that control the structural morphology and pore size of the final membrane films. Thus, an increase in monomer content is anticipated to reduce the time for phase separation. However, it is important to consider that the system's viscosity also plays a role in the kinetics of phase separation. As polymerization progresses, higher viscosity can slow down the dynamics of polymer chains and its diffusion, affecting the rate of phase separation. In systems with lower viscosity, polymers can move more rapidly, which may result in a quicker phase separation process (Fig. 3A).

It has been found that there is a favorable intermolecular ion-dipole interaction between Li<sup>+</sup> cation (in LiTFS) and etheric oxygen [35,36]. Due to these favorable intermolecular interactions between Li<sup>+</sup> and existing oxygens in the structure of BPA-EDMA, the  $\Delta\delta$  and therefore,  $\chi$ were expected to be low leading to enhanced dissolution of BPA-EDMA in the EC/DMMP/LiTFS electrolyte solution. Consequently, it was expected that the LiTFS concentration would influence  $\Delta \delta$  and  $\gamma$ , and therefore, it would affect the PIPS process and the final structural morphology of the membrane. In the absence of LiTFS (M<sub>40</sub>-Li<sub>0.0</sub>, in the LiTFS series, Table 1), the polymerization process increases the systems' free energy, favoring phase separation and a microscale porous structure formation (Fig. 3B). Comparing polymer film with varying levels of Li salt clearly indicated that the presence of LiTFS improves the solubility of monomer and polymer in the EC/LiTFS solution (lower  $\chi$  and  $\Delta\delta$ ) and so delays the phase separation and homogeneous bi-continuous porous structure formation (M<sub>40</sub>-Li<sub>0.0</sub> and M<sub>40</sub>-Li<sub>0.5</sub> and M<sub>40</sub>-Li<sub>1.0</sub> in Fig. 3B) [22]. Further increasing LiTFS (sample M<sub>40</sub>-Li<sub>1.5</sub> with 1.5 M LiTFS) resulted in smaller pore size (Fig. 3B) or even nonporous morphology. We expect this phenomenon to be linked to the increased solubility of the monomer as well as the formed polymer chains, which renders the active vinyl groups more readily available for interaction. This enhances the polymerization kinetics, leading to phase separation at earlier stages. Nevertheless, a more detailed understanding of this process necessitates further in-depth dynamic studies.

#### 3.3. Rheological analysis

Rheological measurements were conducted to examine the impact of monomer and LiTFS contents on the phase separation kinetics. We determined the structural evolution over the polymerization at  $60\,^{\circ}$ C by carrying out the oscillatory time sweep measurements (with an angular frequency of  $10\,$  rad/s and strain of  $0.1\,$ %) and monitoring the storage modulus (G') and loss modulus (G''). A solvent trap was used for all rheological measurements to prevent undesired solvent evaporation (Fig. S2). The phase separation time was defined as the time of the crossover of G' and G'', showing a distinct transition in viscoelastic behavior, changing from liquid-like to solid-like behavior (Fig. 5). This characteristic time, known as gel time, varies with monomer content (Fig. 5A and B) and LiTFS concentration (Figs. 5C, D and S3).

After thermal stabilization, the viscosity shows a consistent increase, particularly in systems with BPA-EDMA > 40 wt%, as indicated by the rising G", aligning with the growth of polymerization in the monomers prior to extensive crosslinked network formation. In this early phase, there is insignificant change in G', with the sample's behavior predominantly influenced by viscous dissipation. However, as time progresses, the elastic response begins to intensify, marked by a rapid increase in G', and surpasses that of G", leading to a crossover point. Our results consistently indicate that the time required for phase separation increases as the monomer content grows up to 60 wt%, likely due to the rising viscosity of the system with more monomer available (Fig. 5A). Typically, a decrease in the system's entropy, caused by a lower solvent fraction, facilitates phase separation. However, the initial increase in viscosity can decelerate the kinetics of phase separation, thus postponing the development of the solid phase. Beyond 60 wt% monomer content, the abundant monomers expedite polymerization and shift the transition to the crosslinked solid phase to shorter time, effectively preventing phase separation (Figs. 5A and B, S1).

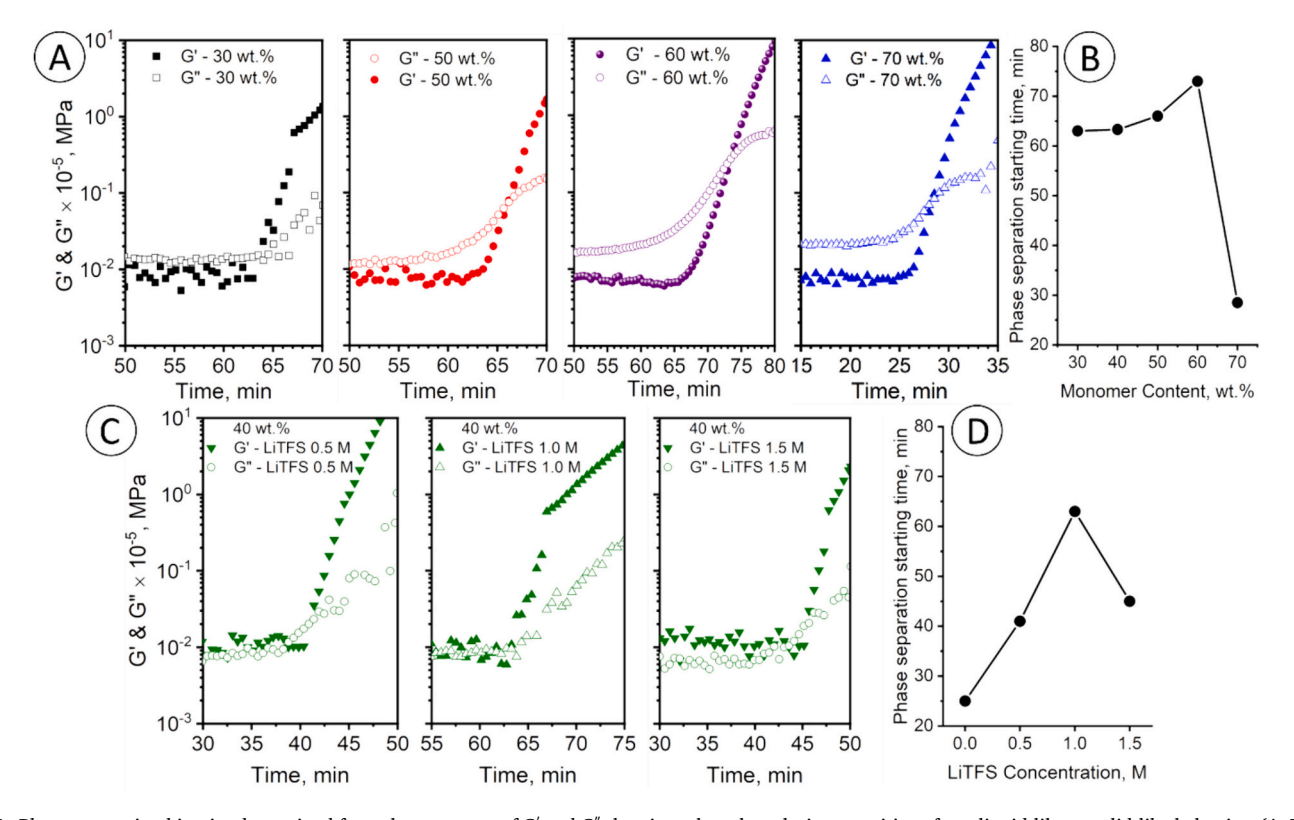


Fig. 5. Phase separation kinetics determined from the crossover of G' and G" showing when the solution transitions from liquid-like to solid-like behavior. (A–B) the effect of monomer content, (C–D) the effect of LiTFS salt content (also see Fig. S3).

The rheological behavior of the liquid electrolytes with various LiTFS amounts (0–1.5 M) was also monitored during the polymerization time. As discussed above, the solubility of monomers and forming polymer chains in EC/LiTFS solution increases with LiTFS content, owing to the favorable intermolecular ion-dipole interactions between Li<sup>+</sup> and oxygen elements present in the monomer and polymer structures. This can decrease  $\Delta\delta$  and  $\chi$ , and reduce the kinetics of the phase separation process. The rheological analysis showed that the onset of phase separation, marked by a sharp rise in G' surpassing G'', enhanced progressively with LiTFS concentration increasing from 0 to 1 M (Figs. 5C and D, S3). Conversely, additional LiTFS (1.5 M) enhanced the polymerization kinetics, advancing the initiation of polymerization and the timing of phase separation to earlier stages, which aligns with our findings from SEM images (Figs. 3B, 5C and D).

#### 3.4. Tensile test results

We performed a uniaxial tensile experiment to understand the correlation between the synthesized HEM films' structural morphology and mechanical performance (Figs. 6, S4). In polymer films with mechanical integrity (monomer content from 40 to 70 wt%), increasing the monomer content was followed by a linear increase in Young's moduli and tensile strength and concurrently resulted in a linear decrease in elongation at break (Fig. 6A and B). This behavior can be attributed to the development of a highly crosslinked solid polymer network. In LiTFS series polymer films, adding LiTFS decreased Young's moduli and tensile strength and increased elongation break (Fig. C and D). This effect can be attributed to the favorable intermolecular interactions between the Li<sup>+</sup> and existing oxygen elements in the polymer structures [35–37]. This interaction results in the incorporation of LiTFS into the polymer network, causing a plasticizing effect and, thereby, lower mechanical

properties. As a result, the HEM films prepared for the sample  $\rm M_{40}\text{-}Li_{1.5}$  did not demonstrate sufficient integration and easily disintegrated during peeling from the glass cells.

## 3.5. Ionic conductivity results

The effect of polymer film microstructure on ionic conductivity was investigated in coin cells for as-synthesized HEMs at three different monomer concentrations (40 wt%, 50 wt% and 60 wt%). The EIS technique was employed to determine the ionic conductivity to obtain the Nyquist plot for each coin cell. Subsequently, the experimental data was fitted using the equivalent circuit from Fig. 2B (inset) to determine the point where the low-frequency part of the curve (to the right) intersects the 0 imaginary impedance and thus calculate the ionic conductivity using Eq. (1). Although the sample containing 40 wt% monomer (M<sub>40</sub>-Li<sub>1 0</sub>) demonstrated larger pores, which was expected to facilitate ion transport, the highest ionic conductivity was surprisingly observed in HEMs with 50 wt% monomer concentration (Fig. 7). Deviating from this specific concentration, either increasing or decreasing it, led to a notable decline in ionic conductivity (Fig. 7). We attribute the higher conductivity of M50-Li1.0 to its optimal balance between structural integrity and pore size. Despite having smaller pores and lower porosity (Fig. 3A), M<sub>50</sub>-Li<sub>1.0</sub> is three times stiffer than M<sub>40</sub>-Li<sub>1.0</sub> (Fig. 6A, B), which helps maintain pore shape and size under the compressive stresses experienced within the coin cell. In contrast, the lower mechanical modulus and greater extensibility of  $M_{40}$ -Li<sub>1.0</sub> (Fig. 6A, B) can lead to structural and porosity deformations, impairing ion transfer and performance. This finding highlights a critical tradeoff between mechanical properties and porosity in porous HEMs, a balance more effectively achieved in M50-Li1.0. While larger pores may potentially improve ion mobility, the mechanical properties of these materials are

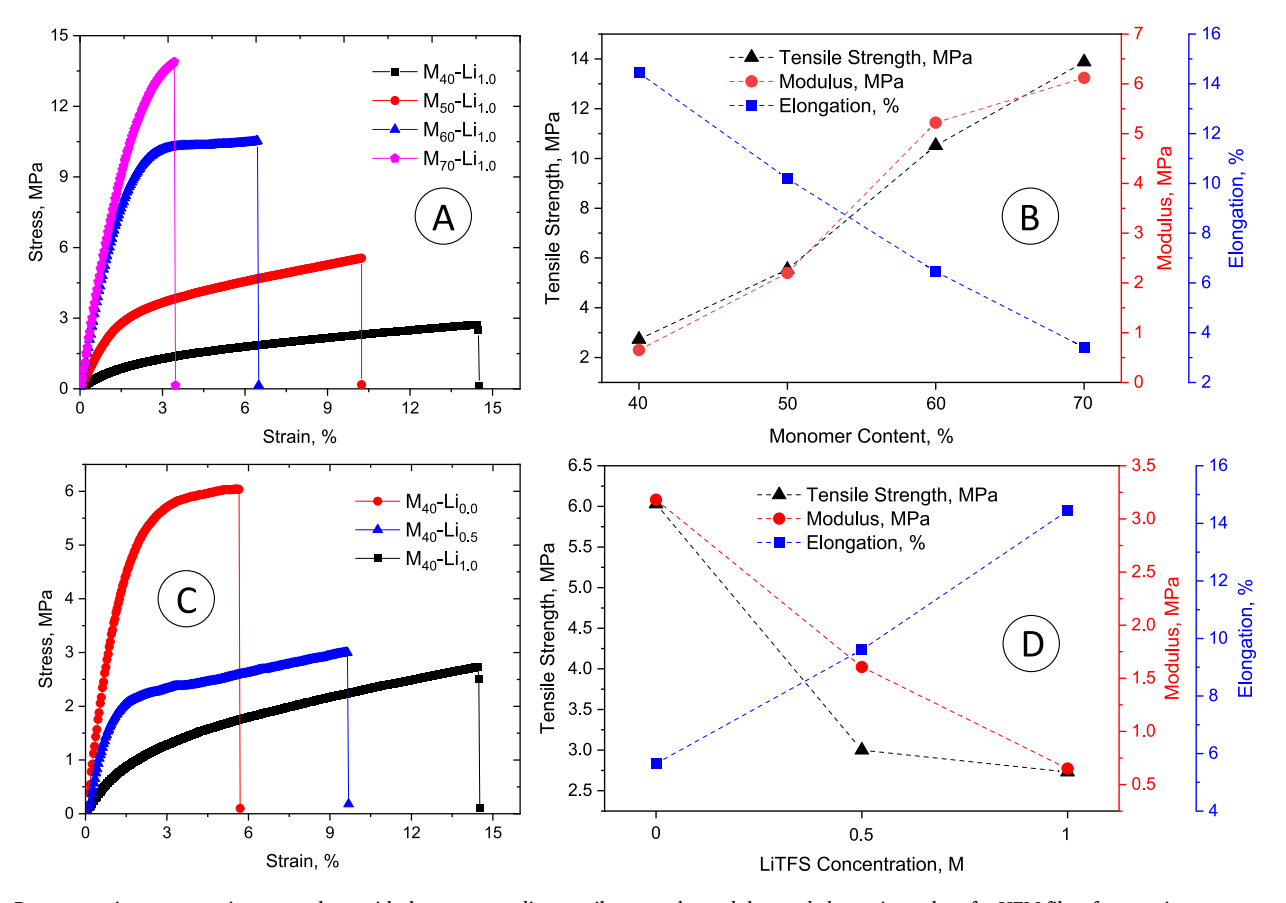
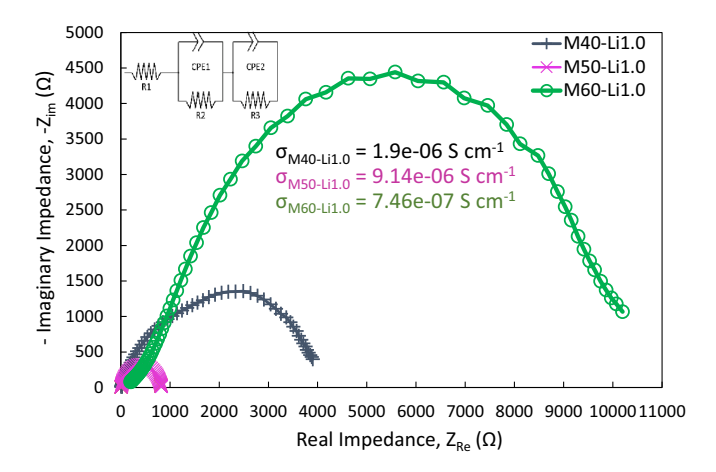


Fig. 6. Representative stress-strain curves along with the corresponding tensile strength, modulus, and elongation values for HEM films from various monomer series (A–B) and LiTFS Series (C–D).



**Fig. 7.** Nyquist plot shows the AC frequency response of the fabricated coin cells containing HEMs prepared with different monomer content.

crucial for maintaining structural stability.

Further exploration into the effects of adding excess liquid electrolytes to the HEMs was conducted, particularly focusing on the formulation with 50 wt% monomer content and 1 M LiTFS. The Nyquist plots, as shown in Fig. S5, compare the ionic conductivity of M<sub>50</sub>-Li<sub>1,0</sub> under varying amounts of an excess EC:DMMP 50:50-Li(1 M) liquid electrolyte solution. Initial measurements of the as-synthesized HEMs presented an ionic conductivity of 9.1·10<sup>-6</sup> S cm<sup>-1</sup> (Fig. S5). Interestingly, the introduction of additional liquid electrolyte solution led to a noticeable, but not very significant, improvement in conductivity. This enhancement can be attributed to the improved wettability between the electrolyte layers, facilitating a more efficient ion transport. When comparing the ionic conductivity of the as-synthesized membrane with the one treated with an additional 20 µL of solution, it also highlights the effectiveness and structural stability of the solid polymer electrolyte (Fig. S5). These aspects are crucial for supporting the electrolyte solution and ensuring the optimal performance of the salt carrier solvent.

## 4. Conclusion

This paper presents a comprehensive experimental analysis of the PIPS phenomenon in the context of preparing porous membranes for use as solid-state electrolyte membranes. Using BPA-EDMA as a monomer and LiTFS as salt, we synthesized heterogeneous electrolyte membrane (HEM) films. Our research meticulously investigated the effects of varying monomer concentrations and LiTFS levels on the ionic conductive properties of these films, utilizing a range of analytical techniques.

Our findings highlight that the ionic conductivity of HEMs is intricately linked to their microstructure, and mechanical properties which are, in turn, influenced by the concentration of monomer and salt. The optimal combination of these components yielded membranes with mechanical strength and pore size crucial for supporting the microstructure and improving ionic conductivity. While the polymer membrane with the highest porosity was attained using 40 wt% of monomer and 1 M LiTFS, its ionic conductivity was considerably lower compared to the membrane with 50 wt%. This disparity is likely due to its insufficient mechanical strength to maintain the microstructure and pore configuration in coin cell setup. Notably, higher monomer content led to denser crosslinked polymer networks, which inversely affected the conductivity. These insights were supported by rheological, SEM, and mechanical characterizations, providing a comprehensive understanding of the factors influencing ionic transport in these materials.

Furthermore, applying Flory–Huggins's mean-field theory provided a valuable theoretical perspective, correlating the experimental observations with the interplay between chemical composition, structural properties, and functional performance. The results from this study significantly contribute to the field of polymer science, particularly in developing advanced materials with tailored ionic conductivities for practical applications.

The implications of our work are far-reaching, particularly in the context of lithium-ion and solid-state batteries, where improved ionic conductivity in solid electrolytes is crucial for enhanced performance, safety, and efficiency.

#### CRediT authorship contribution statement

Nasser Nikfarjam: Writing – original draft, Formal analysis, Data curation, Conceptualization. Paul T. Coman: Writing – original draft, Investigation, Formal analysis, Data curation. Colton Free: Data curation. Paul Ziehl: Validation, Funding acquisition. Monirosadat Sadati: Writing – review & editing, Validation, Supervision, Project administration, Funding acquisition, Conceptualization. Ralph E. White: Supervision, Project administration, Funding acquisition.

## **Declaration of competing interest**

The authors declare that they have no known competing financial interests or personal relationships that could have appeared to influence the work reported in this paper.

## Data availability

Data will be made available on request.

#### Acknowledgments

This work was supported in part by the College of Charleston through the NASA SC Space Grant (Award no. #10013074), NSF-DMR (Award #2146428), NSF REU (Award #2050956) by the SmartState Center for Multifunctional Materials and Structures, and internally through the U of SC Office of the Vice President for Research (ASPIRE-II) (#155100-23-64177).

## Appendix A. Supplementary data

The fabricated HEM films with different BPA-EDMA content, rheological studies of PIPS process at 60  $^{\circ}$ C. Phase separation kinetics determined from the crossover of G' and G" in solutions with different LiTFS content. Tensile experiment set up and the effect of excess electrolyte on the ionic conductivity of HEM M50-Li1.0. Supplementary data to this article can be found online at https://doi.org/10.1016/j.est.20 24.112287.

#### References

- K. Xu, Nonaqueous liquid electrolytes for lithium-based rechargeable batteries, Chem. Rev. 104 (10) (2004) 4303–4418, https://doi.org/10.1021/cr030203g.
- [2] Y. Wang, W.-H. Zhong, Development of electrolytes towards achieving safe and high-performance energy-storage devices: a review, ChemElectroChem 2 (1) (2015) 22–36, https://doi.org/10.1002/celc.201402277.
- [3] S. Li, S.-Q. Zhang, L. Shen, Q. Liu, J.-B. Ma, W. Lv, Y.-B. He, Q.-H. Yang, Progress and perspective of ceramic/polymer composite solid electrolytes for lithium batteries, Adv. Sci. 7 (5) (2020) 1903088, https://doi.org/10.1002/ advs.201903088.
- [4] J.W. Fergus, Ceramic and polymeric solid electrolytes for lithium-ion batteries, J. Power Sources 195 (15) (2010) 4554–4569, https://doi.org/10.1016/j. jpowsour.2010.01.076.
- [5] Z. Xue, D. He, X. Xie, Poly(ethylene oxide)-based electrolytes for lithium-ion batteries, J. Mater. Chem. A 3 (38) (2015) 19218–19253, https://doi.org/10.1039/ C5TA03471J.
- [6] D.E. Fenton, J.M. Parker, P.V. Wright, Complexes of alkali metal ions with poly (ethylene oxide), Polymer (Guildf.) 14 (1973) 589.
- [7] P.V. Wright, Electrical conductivity in ionic complexes of poly(ethylene oxide), Br. Polym. J. 7 (5) (1975) 319–327, https://doi.org/10.1002/pi.4980070505.
- [8] M. Armand, Polymer solid electrolytes an overview, Solid State Ion. 9–10 (1983) 745–754, https://doi.org/10.1016/0167-2738(83)90083-8.

- [9] M. Willgert, M.H. Kjell, E. Jacques, M. Behm, G. Lindbergh, M. Johansson, Photoinduced free radical polymerization of thermoset lithium battery electrolytes, Eur. Polym. J. 47 (12) (2011) 2372–2378, https://doi.org/10.1016/j. euroolymi.2011.09.018.
- [10] N. Ihrner, M. Johansson, Improved performance of solid polymer electrolytes for structural batteries utilizing plasticizing co-solvents, J. Appl. Polym. Sci. 134 (23) (2017). https://doi.org/10.1002/app.44917.
- [11] J.F. Snyder, R.H. Carter, E.D. Wetzel, Electrochemical and mechanical behavior in mechanically robust solid polymer electrolytes for use in multifunctional structural batteries, Chem. Mater. 19 (15) (2007) 3793–3801, https://doi.org/10.1021/ cm0702130.
- [12] M. Willgert, M.H. Kjell, G. Lindbergh, M. Johansson, New structural lithium battery electrolytes using thiol–Ene chemistry, Solid State Ion. 236 (2013) 22–29, https://doi.org/10.1016/j.ssi.2013.01.019.
- [13] A. Manuel Stephan, Review on gel polymer electrolytes for lithium batteries, Eur. Polym. J. 42 (1) (2006) 21–42, https://doi.org/10.1016/j.eurpolymj.2005.09.017.
- [14] N. Shirshova, H. Qian, M. Houllé, J.H.G. Steinke, A.R.J. Kucernak, Q.P.V. Fontana, E.S. Greenhalgh, A. Bismarck, M.S.P. Shaffer, Multifunctional structural energy storage composite supercapacitors, Faraday Discuss. 172 (0) (2014) 81–103, https://doi.org/10.1039/C4FD00055B.
- [15] M. Willgert, S. Leijonmarck, G. Lindbergh, E. Malmström, M. Johansson, Cellulose nanofibril reinforced composite electrolytes for lithium ion battery applications, J. Mater. Chem. A 2 (33) (2014) 13556–13564, https://doi.org/10.1039/ C4TA01139B.
- [16] K. Matsumoto, T. Endo, Confinement of ionic liquid by networked polymers based on multifunctional epoxy resins, Macromolecules 41 (19) (2008) 6981–6986, https://doi.org/10.1021/ma801293i.
- [17] J.F. Snyder, E.D. Wetzel, C.M. Watson, Improving multifunctional behavior in structural electrolytes through copolymerization of structure- and conductivitypromoting monomers, Polymer (Guildf.) 50 (20) (2009) 4906–4916, https://doi. org/10.1016/j.polymer.2009.07.050.
- [18] S. Wang, K. Min, Solid polymer electrolytes of blends of polyurethane and polyether modified polysiloxane and their ionic conductivity, Polymer (Guildf.) 51 (12) (2010) 2621–2628, https://doi.org/10.1016/j.polymer.2010.04.038.
- [19] L.D. McIntosh, M.W. Schulze, M.T. Irwin, M.A. Hillmyer, T.P. Lodge, Evolution of morphology, modulus, and conductivity in polymer electrolytes prepared via polymerization-induced phase separation, Macromolecules 48 (5) (2015) 1418–1428, https://doi.org/10.1021/ma502281k.
- [20] S.A. Chopade, J.G. Au, Z. Li, P.W. Schmidt, M.A. Hillmyer, T.P. Lodge, Robust polymer electrolyte membranes with high ambient-temperature lithium-ion conductivity via polymerization-induced microphase separation, ACS Appl. Mater. Interfaces 9 (17) (2017) 14561–14565. https://doi.org/10.1021/acsami.7b02514.
- [21] N. Ihrner, W. Johannisson, F. Sieland, D. Zenkert, M. Johansson, Structural lithium ion battery electrolytes via reaction induced phase-separation, J. Mater. Chem. A 5 (48) (2017) 25652–25659, https://doi.org/10.1039/C7TA04684G.
- [22] N. Shirshova, A. Bismarck, E.S. Greenhalgh, P. Johansson, G. Kalinka, M. J. Marczewski, M.S.P. Shaffer, M. Wienrich, Composition as a means to control morphology and properties of epoxy based dual-phase structural electrolytes, J. Phys. Chem. C 118 (49) (2014) 28377–28387, https://doi.org/10.1021/ip507052h
- [23] A.J. Manly, W.E. Tenhaeff, One-step fabrication of robust Lithium ion battery separators by polymerization-induced phase separation, J. Mater. Chem. A 10 (19) (2022) 10557–10568, https://doi.org/10.1039/D1TA10730E.

- [24] K. Sakakibara, H. Kagata, N. Ishizuka, T. Sato, Y. Tsujii, Fabrication of surface skinless membranes of epoxy resin-based mesoporous monoliths toward advanced separators for lithium ion batteries, J. Mater. Chem. A 5 (15) (2017) 6866–6873, https://doi.org/10.1039/C6TA09005B.
- [25] Y.H. Song, T. Kim, U.H. Choi, Tuning morphology and properties of epoxy-based solid-state polymer electrolytes by molecular interaction for flexible all-solid-state supercapacitors, Chem. Mater. 32 (9) (2020) 3879–3892, https://doi.org/ 10.1021/acs.chemmater.0c00041.
- [26] L.M. Schneider, N. Ihrner, D. Zenkert, M. Johansson, Bicontinuous electrolytes via thermally initiated polymerization for structural lithium ion batteries, ACS Appl. Energy Mater. 2 (6) (2019) 4362–4369, https://doi.org/10.1021/ acsaem.9b00563.
- [27] M. Cattaruzza, Y. Fang, I. Furó, G. Lindbergh, F. Liu, M. Johansson, Hybrid polymer-liquid lithium ion electrolytes: effect of porosity on the ionic and molecular mobility, J. Mater. Chem. A 11 (13) (2023) 7006–7015, https://doi.org/ 10.1039/D3TA00250K
- [28] N. Peruzzi, B.W. Ninham, P. Lo Nostro, P. Baglioni, Hofmeister phenomena in nonaqueous media: the solubility of electrolytes in ethylene carbonate, J. Phys. Chem. B 116 (49) (2012) 14398–14405, https://doi.org/10.1021/jp309157x.
- [29] J.W. Barlow, P.E. Cassidy, D.R. Lloyd, C.-J. You, Y. Chang, P.C. Wong, J. Noriyan, Polymer sorbents for phosphorus esters: II. Hydrogen bond driven sorption in fluoro-carbinol substituted polystyrene, Polym. Eng. Sci. 27 (10) (1987) 703–715, https://doi.org/10.1002/pen.760271003.
- [30] M. Benz, S.V. Patel, Freestanding chemiresistive polymer composite ribbons as high-flux sensors, J. Appl. Polym. Sci. 125 (5) (2012) 3986–3995, https://doi.org/ 10.1002/app.36538
- [31] S.I. Abdul Halim, C.H. Chan, J. Apotheker, Basics of teaching electrochemical impedance spectroscopy of electrolytes for ion-rechargeable batteries – part 1: a good practice on estimation of bulk resistance of solid polymer electrolytes 3 (2) (2021) 105–115, https://doi.org/10.1515/cti-2020-0011.
- [32] S. Zheng, L. Wei, Z. Zhang, J. Pan, J. He, L. Gao, C.C. Li, In situ polymerization of ionic liquid with tunable phase separation for highly reversible and ultralong cycle life Zn-ion battery, Nano Lett. 22 (22) (2022) 9062–9070, https://doi.org/ 10.1021/acs.nanolett.2c03421.
- [33] M. Rubinstein, R.H. Colby, Polymer Physics, Oxford University Press, London, 2003
- [34] K. Kanamori, K. Nakanishi, T. Hanada, Rigid macroporous poly(divinylbenzene) monoliths with a well-defined Bicontinuous morphology prepared by living radical polymerization, Adv. Mater. 18 (18) (2006) 2407–2411, https://doi.org/10.1002/ adma.200601026.
- [35] H.K. Jang, B.M. Jung, U.H. Choi, S.B. Lee, Ion conduction and viscoelastic response of epoxy-based solid polymer electrolytes containing solvating plastic crystal plasticizer, Macromol. Chem. Phys. 219 (6) (2018) 1700514, https://doi.org/ 10.1002/macp.201700514.
- [36] B. Park, T. Kim, S. Jeon, S.J. Kwon, H.K. Jang, B.M. Jung, S. Ahn, U.H. Choi, J. Lee, S.B. Lee, Influence of intermolecular interactions on molecular geometry and physical quantities in electrolyte systems, Mol. Phys. 117 (14) (2019) 1790–1795, https://doi.org/10.1080/00268976.2018.1543905.
- [37] R. He, T. Kyu, Effect of plasticization on ionic conductivity enhancement in relation to glass transition temperature of crosslinked polymer electrolyte membranes, Macromolecules 49 (2016) 5637–5648.